Physics of Plasmas

Non-local plasma generation in a magnetic nozzle

Cite as: Phys. Plasmas **26**, 072107 (2019); https://doi.org/10.1063/1.5098484
Submitted: 02 April 2019 . Accepted: 14 June 2019 . Published Online: 19 July 2019

Alexander Bennet, Christine Charles, and Rod Boswell

Physics of Plasmas ARTICLE scitation.org/journal/php

Non-local plasma generation in a magnetic nozzle

Cite as: Phys. Plasmas **26**, 072107 (2019); doi: 10.1063/1.5098484
Submitted: 2 April 2019 · Accepted: 14 June 2019 ·
Published Online: 19 July 2019

Alexander Bennet,[a] Christine Charles, and Rod Boswell

AFFILIATIONS

Space Plasma, Power and Propulsion Laboratory, Research School of Physics and Engineering, The Australian National University, Canberra, ACT 2601, Australia

[a]Email: alex.bennet@anu.edu.au

ABSTRACT

Axial plasma density measurements in a 1.5 m long plasma chamber are presented for when the regions of high magnetic field and radio frequency heating are progressively separated using a movable solenoid pair. The results show that the operating regime changes based on the degree of ion magnetisation under the antenna. When ions are magnetized, electrons heated under the antenna are efficiently transported to the solenoids along a column defined by the magnetic field lines which connect to the antenna region. The cross section of this column decreases due to the converging magnetic field geometry, thereby increasing the density of electrons on the axis. This results in a density profile which is singly peaked and centered on the location of maximum magnetic field strength. When the ions are unmagnetised under the antenna, the flux of positive charges to the wall there is increased. Electrons streaming along field lines that intersect the radial wall in the antenna region are then more attracted to the antenna region to balance this flux. This affects the equilibrium conditions along the entire magnetic field line and results in less efficient transport of electrons heated by the antenna to the region of high magnetic field strength. In this regime, there is a global decrease in plasma density and the axial density profile is doubly peaked.

I. INTRODUCTION

The behavior of high density plasmas in nonuniform magnetic fields is of great interest to the astrophysical, fusion, and propulsion communities. For fusion, high density plasma sources can be used to investigate fusion relevant turbulence effects[1,2] and instabilities,[3] and test plasma-facing materials,[4,5] and are being investigated for uncaesiated negative ion production for neutral beam injection systems.[6] In space propulsion, magnetic nozzles have been shown to generate electric fields and induce the creation of current-free double layers in expanding plasmas which contribute to ion beam formation and collimation. Apart from being intrinsically interesting, these effects are useful for generating thrust.[7–10] Magnetic nozzles themselves are ubiquitous in nature, both in the terrestrial and astrophysical plasmas, being a characteristic of most magnetic dipoles immersed in a plasma. The terrestrial plasma experiments mentioned above are dominated by gradients in magnetic fields, typically at the ends of linear systems, in expanding plasma devices and pose significant challenges for the stability of toroidal reactors used in fusion research. In the analysis of such systems, it is natural to consider a spatially localized source of plasma and then consider what happens when it encounters a nonuniform magnetic field. In this situation, plasmas produced using helicon waves yield some of the highest densities known and have been studied extensively in laboratory plasmas with uniform and nonuniform magnetic fields.[11–15] Many astrophysical situations best resemble a magnetic bottle or funnel with examples being the origin of the solar wind on the Sun's photosphere[16] (and references therein), the polar regions of the Earth and Jupiter, and compact objects such as neutron stars.[17–19] However, there is a great difference in where the source of the plasma is relative to the magnetic field; on the Sun, it is in the throat of the nozzle and in polar regions of planets in the weak regions of the magnetic field expansion, far from the dipole.

Many linear devices use converging magnetic fields to axially contain plasmas via adiabatic reflection. However, when a plasma source is located on the axis but somewhat distant from a magnetic nozzle, in certain cases, the plasma density has been shown to increase the magnetic field gradient.[20] This observation has led to some debate on the forces in play and whether simple fluid concepts like the Boltzmann equation can be usefully employed in trying to understand the system. As most of the experiments were not designed to expressly study this behavior, the present study reports plasma measurements in a newly purpose built reactor which features a 1.5 m long glass tube where a solenoidal magnetic field and a radio frequency (RF) generated plasma source can be progressively separated. Therefore, this study focuses on the behavior of a low pressure RF plasma incident on a remote, converging-diverging magnetic nozzle.

II. ECHIDNA EXPERIMENTAL SETUP

This work is conducted in the new plasma reactor depicted in Fig. 1 and named Echidna for its long "snout." The vacuum system consists of a 1.5 m long, 4.5 cm inner radius borosilicate glass tube attached contiguously to a 60 cm long, grounded aluminum 6-way cross vacuum chamber connected to a 400 l/s turbo-molecular rotary pump combination resulting in a base pressure of between 10^{-7} and 10^{-6} Torr measured with an ionization gauge. The other end of the glass tube is terminated with a grounded aluminum end plate which features a custom-made VacuumSlide, allowing for both radial and axial articulation of *in situ* diagnostic probes.[21] Argon gas is introduced into the system at the pumping end with the flow rate being controlled using a mass flow controller while operating pressures are measured using a Baratron gauge in the 50 mTorr range located at the pumping end. Pressure measurements have been conducted with a Baratron at both ends of the experiment and have shown that there is no pressure gradient along the glass tube. The origin of the coordinate system, i.e., $(z, r) = (0, 0)$ cm, used in this study is defined at the center of a 19 cm long double saddle antenna[13] which is situated 50 cm from the interface with the 6-way cross vacuum chamber. The antenna is fed with RF power at 13.56 MHz through an L-matching network and spans the axial region $-9.5 \leq z \leq 9.5$ cm. A pair of solenoids is mounted concentrically with the glass tube on a movable platform which allows for arbitrary axial positioning of the magnetic field, and the axial location of the center of the solenoid pair is defined as z_B, as illustrated in Fig. 1. Each solenoid consists of 130 windings of 4 cm wide and 0.5 mm thick copper strap cowound with a 0.2 mm thick insulator and is supplied with a current, I_{sol}, by a high current power supply, providing maximum axial magnetic field strengths of ~7.5 G/A up to about 1 kG. Computationally calculated field lines generated by the solenoids are also shown in the figure for $z_B = -30$ cm. For these experiments, a thin grounded aluminum sleeve was inserted into the glass tube such that the region between $z = -15$ cm and the 6-way cross has a grounded radial boundary. This was introduced to provide a defined ground close for the plasma under the antenna. Without it, the plasma was unstable and flickered between being connected to the grounded pumping port and residing just under the antenna. Regions where the radial boundary is grounded have been shaded in gray in Fig. 1.

III. DIAGNOSTICS

The diagnostic probes used in this study are inserted via the VacuumSlide at the $z = -100$ cm end of the glass tube and mounted at an angle to their grounded aluminum probe shafts which are radially offset from the axis by 3.5 cm, as shown in Fig. 1. This allows for a significant reduction in plasma perturbation as the probe tip is moved through the regions of high plasma density. The *in situ* probes used here consist of an uncompensated Langmuir probe (LP), a RF-compensated Langmuir probe (CP), an emissive probe (EP), and a B-dot probe. The LP consists of a one-sided planar nickel disk with a radius of 0.95 mm and is biased to −80 V to measure the local ion saturation current, I_{sat}, which is used to calculate the local ion density using the simple relation: $I_{sat} \simeq 0.6 q A_p c_s n_i$, where q is the elementary charge, A_p is the probe tip, c_s is the local ion sound speed, and n_i is the ion density.[22,23] The CP follows a design published previously,[24] consists of a 0.5 mm diameter, 5 mm long cylindrical tungsten tip aligned perpendicularly to the magnetic field lines, and measures the electron energy probability function (EEPF) through the implementation of analog differentiator circuits.[25,26] When measuring directly under the solenoids, the electron Larmor radius is on the order of, or smaller, than the probe tip radius and the first derivative of the probe's I-V trace is used to determine the EEPF.[27,28] When the field is low and the

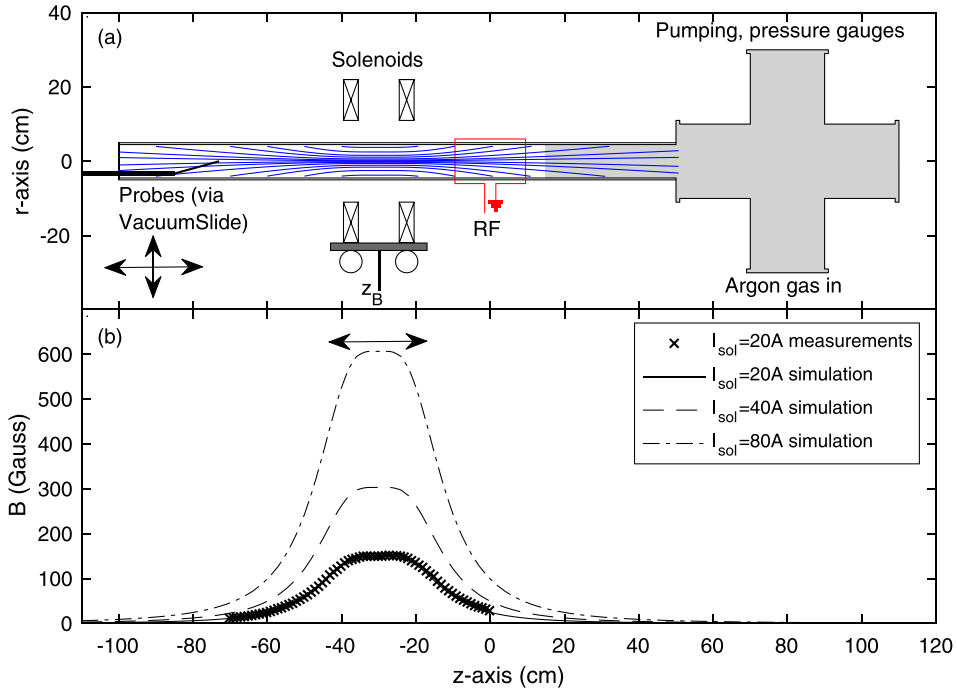

FIG. 1. (a) Schematic of the Echidna reactor showing the borosilicate glass tube ($z < 50$ cm), the 6-way cross vacuum chamber ($z > 50$), and the locations of the RF antenna, vacuum pump connections, pressure gauges, argon gas inlet, and diagnostic probes inserted via the VacuumSlide. Regions where the radial wall is grounded are shaded in gray. Probes are inserted from the end at $z = -100$ cm and are mounted on a dog leg such that the probe shaft does not disturb the plasma on the axis. The solenoid pair is centered on z_B and can be moved along the axis. The calculated magnetic field lines are plotted for the depicted position of the solenoids ($z_B = -30$ cm), showing the converging-diverging nature of the field. The B-field strength on the axis for $I_{sol} = 20$, 40, and 80 A is plotted in (b) and measurements of the $I_{sol} = 20$ A case closely align with the simulated field strength.

electrons are less strongly magnetized, the second derivative of the I-V trace is used, as per the normal Druyvesteyn method for unmagnetised plasmas.[29] The slope of the EEPF on a semilog plot is used to determine the electron temperature, T_e. The EP consists of a ∼5 mm long thoriated tungsten coil supplied with current from a DC power supply and uses the floating potential method to measure the local plasma potential, V_p.[30] The B-dot probe consists of a 0.25 mm diameter enameled copper wire wound into a 7 turn magnetic pickup coil 4 mm in diameter, similar to that presented in Ref. 31. The coil is housed inside a glass pipette, ensuring that the probe does not directly contact the plasma. Both ends of the copper wire are wound through an iron toroid to form a hybrid combiner which reduces electrostatic pickup due to capacitive coupling from the RF antenna and plasma to the probe tip, allowing for direct measurement of RF magnetic fields in the plasma.[32] The B-dot probe was mounted such that it would measure the radial component of the RF magnetic fields, B_r, throughout the chamber. The B-dot probe was tested without a plasma present by measuring B_r near an azimuthal strap of the double saddle antenna and measured the correct direction of the RF magnetic field without electrostatic interference from RF electric fields.

IV. AXIAL AND RADIAL CHARACTERISTICS

To characterize the plasma behavior when the solenoidal magnetic field is moved away from the RF antenna, the experiment was run with an argon fill pressure of 1 mTorr, a relatively low RF power of 200 W and a solenoid current of 40 A, producing a magnetic field with a maximum axial strength of around 300 G (Fig. 1). By sweeping the RF power in the range of 200 W–500 W and holding the other experimental conditions constant, the plasma density at $z = 0$ cm (not shown here) was seen to increase approximately linearly with increasing RF power which implies that the system is operating in an inductively coupled mode.[33] Axial profiles of the local ion density were collected from $z = -80$ cm to $z = 10$ cm in 2 cm increments with the LP for varying positions of the solenoids. Figure 2 shows the density profiles for values of z_B varying from $z_B = 0$ to $z_B = -60$ cm in 10 cm increments. Also shown in Fig. 2 is the region directly under the antenna shaded in gray and the location of z_B as a vertical dashed line. When calculating the ion densities, a measured T_e of 5 eV is used to determine the local ion sound speed for the 1 mTorr case (discussed later). For $z_B = 0$ cm, the solenoids are positioned directly over the antenna and the axial density profile exhibits a single peak value of $\sim 4.5 \times 10^{11}\,\mathrm{cm}^{-3}$ aligning with the center of both the solenoids and the antenna. The density decreases away from this peak as the magnitude of the magnetic field decreases in a manner closely proportional to the strength of the magnetic field.

Interestingly, the position of peak density follows the movement of the solenoids as they are moved from $z_B = 0$ cm to $z_B = -30$ cm. As can be seen in Fig. 2, the singly peaked axial density profile centered around the value of z_B also increases as the solenoids and antenna are separated and is maximum at $z = z_B = -30$ cm where $n_i \sim 9 \times 10^{11}\,\mathrm{cm}^{-3}$. However, this behavior changes when the solenoids are moved further away from the antenna region. The figure shows that for values of $z_B = -40, -50, -60$ cm the density profiles appear to have split into two local density maxima: one which is centered on z_B and one that is localized to the antenna region. Both density maxima decrease in magnitude with increasing separation between the solenoids and antenna.

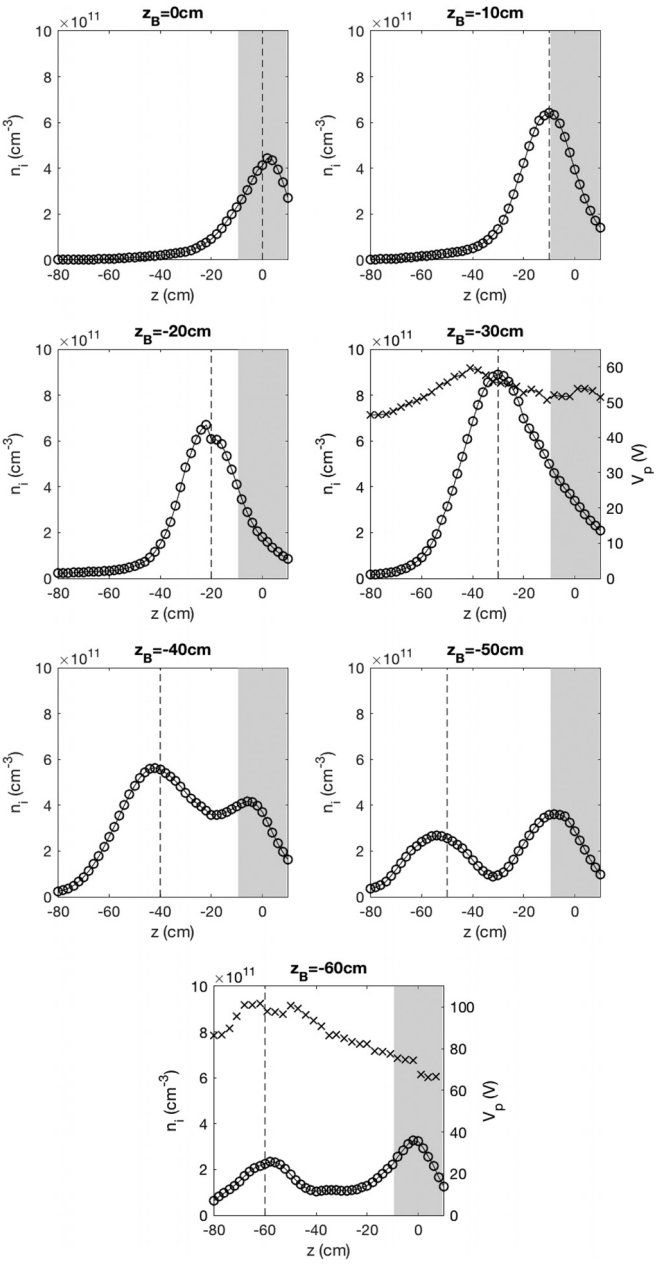

FIG. 2. Axial density measurements for different values of z_B for experimental conditions of 1 mTorr, 200 W RF power, and $I_{sol} = 40$ A. Measurements of the axial plasma potential are shown as crosses in the $z_B = -30$ cm and $z_B = -60$ cm cases. The region directly under the RF antenna is shaded in gray, and the location of z_B is indicated by the vertical dashed line.

Figure 2 indicates that the axial density behavior can be described by two separate regimes. In the first regime, when the solenoids are positioned within 30 cm of the antenna, the density profile is entirely centered on z_B. In the second regime, the solenoids are positioned further away from the antenna and the plasma is characterized by two local maxima centered on z_B and the antenna. It is interesting to

examine the transition between these two regimes, exploring the mechanism behind the large increase in plasma density on the axis exhibited in the $z_B = -30$ cm case and attempting to understand why the density decreases beyond this point.

First, the plasma transport in the $z_B = -30$ cm case is investigated to better understand why the plasma density is a maximum at the remote solenoids. Also shown in the $z_B = -30$ cm plot in Fig. 2 is the axial plasma potential measured using the EP. The plasma potential demonstrates a peak value of 60 V in the region of the solenoids. Under the antenna, $V_p \sim 53$ V, yielding an increase in a plasma potential of about 7 V from the antenna to solenoid. This would generate an axial electric field that would act to accelerate electrons toward the solenoids while repelling ions which could be a possible mechanism of how electrons might be transported to the solenoids as the electric field would tend to balance the effect of adiabatic reflections caused by the strong magnetic mirror ratio present in the system when the solenoids are far from the antenna. An analysis of the relative strength of the ambipolar electric field compared to the magnetic mirror force can be undertaken to determine if either is dominating the plasma dynamics. The magnetic mirror force, F_B, acting to oppose the velocity of an electron moving toward the magnetic field from the $+z$ direction is given by equation 1 (Ref. 34) while the electrostatic force in the $-z$ direction due to the ambipolar electric field is simply $F_E = qE$, where E is the magnitude of the ambipolar electric field in the $-z$ direction

$$F_B = \frac{1}{2}\frac{mv_\perp^2}{B}\left|\frac{\partial B}{\partial z}\right|, \tag{1}$$

where $v_\perp$ is the electron velocity perpendicular to the magnetic field lines and B is the magnetic field strength. By setting $v_\perp = v_{th}$ where v_{th} is the thermal velocity of electrons, the maximum mirror force on the axis can be found for the case where $I_{sol} = 40$ A and is $F_B \sim 3.7 \times 10^{-18}$ N in the $+z$ direction. The measured potential profile indicates an increase of 7 V from the antenna to solenoids for the $z_B = -30$ cm case. This represents an average electric field of 23 V/m and the average force on an electron is $F_E \sim 3.7 \times 10^{-18}$ N in the $-z$ direction. Given that $F_E \sim F_B$, it appears that the ambipolar electric field is set up to balance the maximum magnetic mirror force on the electrons in this case.

For the $z_B = -30$ cm case, the magnitude of the potential variation along the axis is on the order of T_e and the structure would drive ion diffusion away from the solenoids in both axial directions. On the far side of the solenoids from the antenna, the plasma potential decreases to less than 50 V by $z = -65$ cm and would therefore repel electrons. Applying the Boltzmann equation directly to axial profiles here is difficult given that there is probably local ionization occurring between the antenna and solenoids; however, the close coincidence of the maximum density and potential appears to be acting in a Boltzmann-like way. Figure 2 also shows the axial plasma potential profile for the $z_B = -60$ cm case, i.e., a case which is seen to operate in the regime with two density peaks. Again, the potential profile is peaked under the solenoids, showing a maximum potential of ~100 V which decreases axially to about 75 V near the RF antenna. Interestingly, the maximum plasma potential aligns with the density peak located under the solenoids meaning that the Boltzmann relation appears to apply in the solenoid region but not close to the antenna. Further investigation of the particle transport in this second operating regime will be conducted in future studies and the rest of this paper will focus on the high density regime and why there is a regime transition.

To further investigate the behavior of the $z_B = -30$ cm case, the LP and CP are used to measure the radial profiles of n_i, T_e, and V_p at $z = z_B$ in radial increments of 0.5 cm. The radial data for $z = z_B = -30$ cm (triangles) are compared with the equivalent data taken for the $z = z_B = 0$ cm case (circles) in Fig. 3. The vertical dashed line shown in Fig. 3 corresponds to the radial position of the most radial magnetic field line that intersects with the closest end of the antenna region for the $z = z_B = -30$ cm case and has no particular significance when considering the $z_B = 0$ cm data. In Fig. 3(a), the density data at $r = 0$ cm show the same increase in axial density that was seen when moving the solenoids from $z_B = 0$ cm to $z_B = -30$ cm in Fig. 2. In the $z_B = 0$ cm case, the density decreases radially from 4.2×10^{11} cm^{-3} on the axis to 2.7×10^{11} cm^{-3} at $r = 4$ cm, a reduction of 35%. In the $z_B = -30$ cm case, the density is also seen to be lower at the wall; however, there is a distinct peak off-axis at approximately the same radial location as the most radial magnetic field line to intersect with the antenna. This density peak at $r \sim 3$ cm has approximately the same magnitude as that on the axis, $\sim 8.5 \times 10^{11}$ cm^{-3}. It is unclear what creates this off-axis density peak; however, it could be related to the radial potential profiles discussed below.

Figure 3(b) shows the radial values of T_e measured by the CP for both positions of the solenoids. The EEPFs measured in this study were characterized by single-temperature Maxwellian distributions, consistent with those observed in a similar device in Ref. 20. The profiles show similar electron temperatures of about 5 eV on the axis, most likely because the pressure is unchanged. For the $z_B = 0$ cm case, the electron temperature peaks off axis with an increase in T_e of about 1.5 eV, centered around approximately $r = 2.5$ cm. For a density of $\sim 3 \times 10^{11}$ cm^{-3} here, the radial RF skin depth, calculated using the simple formula $\delta_{RF} = c/\left(2\pi 9000\sqrt{n_i}\right)$, where c is the speed of light in vacuum, is approximately 1 cm. The increase in T_e radially could therefore be due to the RF power being more effectively absorbed by the plasma within the first few skin depths from the radial wall. The electrons here are highly magnetized and would not be able to diffuse inwards to the center, meaning that they would not thermalise across the magnetic field lines. For the $z_B = -30$ cm case, the radial T_e demonstrates different behaviors and drops by more than a factor of 2 from the center to the edge. The decrease in T_e from 5 eV to 2 eV occurs at approximately the same radial position as the most radial magnetic field line to intersect the antenna region. The CP was also used to measure the electron temperature at $z = 0$ cm, $r = 0$ cm in the $z_B = -30$ cm case, and the electron temperature was also found to be 5 eV. Therefore, the electrons heated by the RF antenna appear to be funneled axially through the experiment to the region of high magnetic field strength along the magnetic field lines that pass through the antenna region. These heated electrons would be accelerated by the DC ambipolar field discussed earlier and plotted in Fig. 2 for the $z_B = -30$ cm case. Radially outside the magnetic field lines that pass through the antenna, a colder electron population is present because these cannot access the RF heating region.

Figure 3(c) shows the radial profiles of V_p measured by the CP for the two values of z_B considered here. In both cases, the radial potential profile is of similar magnitude (~60 V) and is remarkably flat, showing that there are no large radial electric fields under the solenoid. The inset in Fig. 3(c) shows the same data zoomed in showing

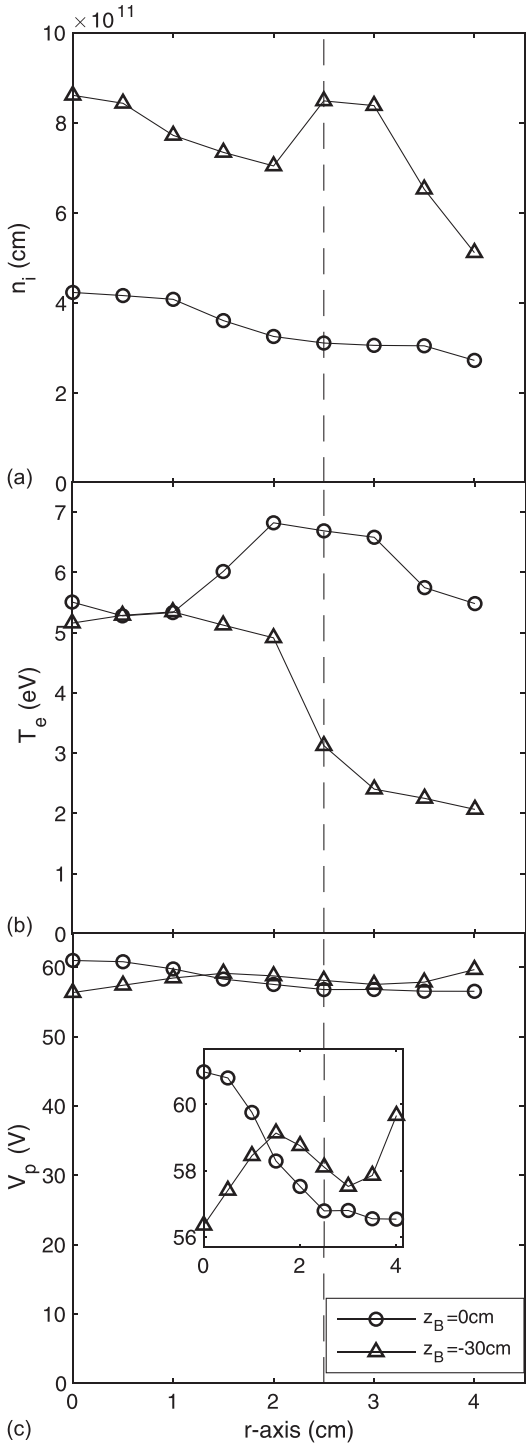

FIG. 3. Radial measurements of (a) ion density, n_i, (b) electron temperature, T_e, and (c) plasma potential, V_p, under the solenoids (i.e., $z = z_B$) for $z_B = 0$ cm (circles) and $z_B = -30$ cm (triangles). The dashed vertical line is the location of the most radial magnetic field line that passes through the antenna region for the $z_B = -30$ cm case. The inset in (c) shows the same radial V_p data but is zoomed in on the y-axis, allowing for the smaller scale structure to be seen.

that there is actually some structure in these profiles and that small radial electric fields are generated. In the $z_B = 0$ cm case, the potential profile is centrally peaked, decreasing from an axial value of 61 V to 56 V at $r = 4$ cm. Again, this potential structure is on the order of T_e and would serve to eject ions radially from the plasma. In the $z_B = -30$ cm case, the profile is reversed with a maximum V_p of 59.5 V found at $r = 4$ cm and a minimum of 56 V on the axis. Such a structure would act to radially confine ions in the plasma, even if only by a potential of 4 V. The figure also shows a local V_p maximum at $r = 1.5$ cm and a local minimum at $r = 3$ cm. For the region $r < 1.5$ cm, ions would be accelerated to the center by this radial potential structure while electrons would be pushed toward the local maximum at $r = 1.5$ cm; however, the cross field transport of these magnetized electrons is expected to be minimal. For $r > 1.5$ cm, the structure would trap ions in the potential well at $r = 3$ cm, while electrons would either be accelerated to $r = 1.5$ cm or the radial wall. The potential well could explain why there is an off-axis density peak at a similar radial location in the $z_B = -30$ cm data in Fig. 3(a). The potential well itself could be a result of the radial drop in electron temperature which would cause a radial electron pressure gradient straddling the most radial field line to pass through the antenna region. It should be noted, however, that the variations in the radial potential profiles are very small when compared to the total magnitude of the measured V_p.

In Fig. 3(c), the radial profiles are very flat, indicating that there is probably significant charging of the radial wall. This is true even where the electron temperature decreases suggesting that the floating potential, V_f, changes such that the relation $V_p - V_f \sim 5kT_e$, where k is the Boltzmann constant, remains true for constant V_p. Indeed, measurements of the floating potential taken with the LP (not shown here) demonstrate a minimum in the center and increase toward the walls, similar to those shown previously.[20]

The results presented here provide valuable insight into how the plasma is formed under the solenoids. The radial profiles of T_e indicate that only electrons from the area defined by the magnetic field lines that pass through the antenna region will contribute significantly to local ionization at the distant solenoid. The velocity of these electrons would mostly be parallel to the magnetic field lines due to the axial potential profile which peaks near the solenoids. As the electrons heated under the antenna flow toward the solenoids, the converging magnetic field geometry increases their density due to the geometry of the most radial field line which intersects the antenna. Given that this field line is located at $r = -2.5$ cm for $z = z_B = -30$ cm and the inner radius of the glass tube is 4.5 cm, the column of electrons transported to the solenoids would decrease in area by a factor of $4.5^2/2.5^2 \sim 3.2$. As such, the density would be expected to increase by this ratio. Examining the axial density profile for the $z_B = -30$ cm case in Fig. 2 and comparing the density at $z = -30$ cm to that at $z = 0$ cm yields an axial increase by a factor of about 2.7, similar to that expected from the magnetic field topology.

Under the solenoid, the mean free path for ion-neutral charge exchange collisions, $\lambda_i \sim 2.5$ cm, is larger than the ion Larmor radius for ions with a thermal velocity of 400 m/s, $r_{Li} \sim 0.5$ cm, meaning that an ion will, on average, collide each time it completes an orbit around a field line. Given that the radial plasma potential is flat and the radial density profile does not follow the radial T_e profile, it suggests that the gyro radius and collisions determine the radial ion dynamics.

V. DEPENDENCE ON RF POWER AND PRESSURE

Now that the behavior of the $z_B = -30$ cm case has been established relative to the $z_B = 0$ cm case, the factors that determine the value of z_B at which there is a regime change can be investigated, as discussed earlier in relation to the axial density profiles. The results presented in Figs. 2 and 3 showed that prior to this regime change, the density was maximum on the axis due to the radial contraction of the plasma column through which electrons are transported to the region of high magnetic field. For $|z_B| > 30$ cm, this electron transport is not very efficient and results in the two regions of density seen earlier. To identify why this might be, the dependence of the plasma behavior on RF power and pressure was investigated by increasing the power to 500 W and varying the pressure over an order of magnitude from 0.5 to 5 mTorr.

Figure 4 shows the axial density profiles when z_B is moved from 0 cm to −60 cm, measured with the LP during experiments run with pressures of 0.5, 1, and 5 mTorr, an RF power of 500 W, and a solenoid current of 40 A. With an increase in power from 200 W to 500 W, the peak density on the axis in the 1 mTorr, $z_B = -30$ cm case has increased to over 10^{12} cm^{-3} and a blue core (argon ion emission lines) can be seen under the solenoids. In a similar manner to that discussed in Sec. VI, the density profiles exhibit a single peak under the solenoids for positions of $|z_B| < 30$ cm. When the separation between the solenoids and antenna is increased, the same transition from a singly peaked density profile to a doubly peaked profile is observed. This indicates that this behavior is independent of the RF power in this range. Higher RF powers were not explored because the experiments were run in a continuous mode and higher density plasmas would probably damage the probes used. Future experiments operated in a pulsed mode could be done to explore if this trend holds for higher powers, e.g., in the kW range.

The existence of a high density plasma and a blue core is commonly associated with the propagation of helicon waves in similar RF plasmas. To investigate whether this is the case in Echidna, the B-dot probe was swept along the central axis where the maximum B_r would be expected for a propagating m = 1 helicon wave mode. Disappointingly, no helicon wave fields were detected under any of the experimental conditions discussed in this study. But alas, the moving probe measures and having measured moves on. Furthermore, no resonances in the system were observed as the solenoids were separated from the RF antenna and the magnetic field strength at $z = 0$ cm approached values where Doppler shifted cyclotron resonance heating of electrons perpendicular to the field lines has been observed previously.[35] Therefore, it appears that wave related heating effects are negligible under the current experimental conditions.

As well as being invariant to changes in RF power (i.e., comparison between the 1 mTorr case in Fig. 4 and the results in Fig. 2), the axial density behavior shown in Fig. 4 appears to be invariant under changes in argon pressure. Figure 4 shows that for increasing separation of the solenoids and the antenna, the axial profiles show a maximum density in the $z_B = -30$ cm case for all pressures. Here, measured T_e values of 6.4 and 3.3 eV were used for the 0.5 mTorr and 5 mTorr cases, respectively, when calculating the density. The axial behavior for different values of z_B can be described in the same way as previously, i.e., single peak for $|z_B| < 30$ cm and double peak with decreasing density for $|z_B| > 30$. This implies that the mean free path for collisions of any type is not the determining factor for the critical

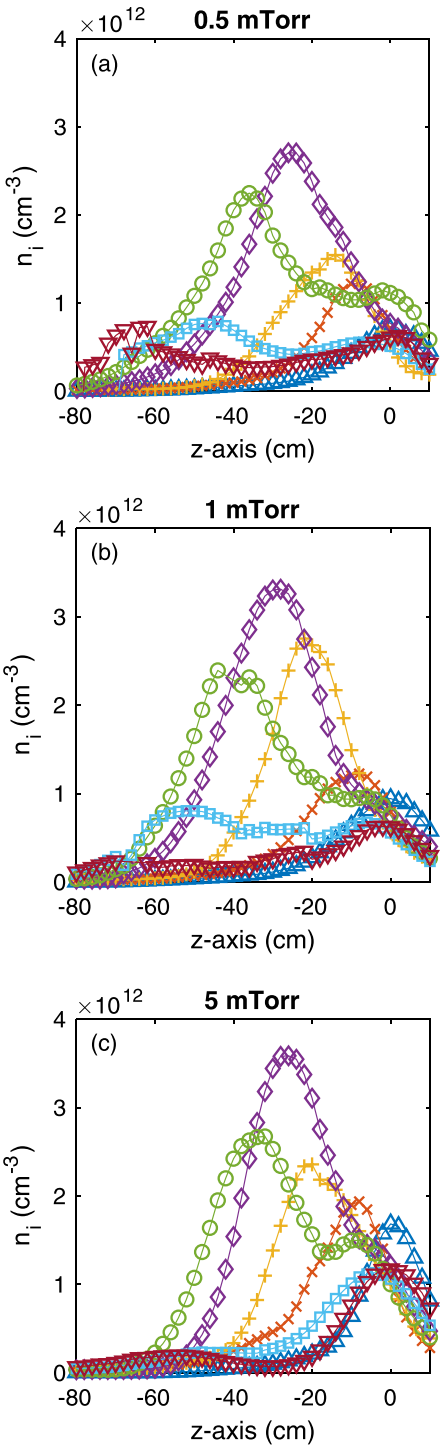

FIG. 4. Axial plasma density measurements experimental conditions of 500 W RF power, $I_{sol} = 40$ A, and argon pressures of (a) 0.5 mTorr, (b) 1 mTorr, and (c) 5 mTorr. The solenoids were positioned at locations of $z_B = 0$ cm (blue upward pointing triangles), $z_B = -10$ cm (orange crosses), $z_B = -20$ cm (yellow plus signs), $z_B = -30$ cm (purple diamonds), $z_B = -40$ cm (green circles), $z_B = -50$ cm (light blue squares), and $z_B = -60$ cm (dark red downward pointing triangles).

value of z_B which determines the regime change. It should be noted however that for the $z_B = -50, -60$ cm cases at 5 mTorr, the density peak at $z = z_B$ is very low compared to that at 0.5 mTorr, suggesting that the plasma ionization far from the antenna is inhibited at high pressures. Therefore, it seems that the remote ionization occurring under the solenoid for large values of $|z_B|$ is dependent on the pressure as the mean free path of collisions decreases and electrons cannot be transported as efficiently to the solenoids.

VI. DEPENDENCE ON MAGNETIC FIELD STRENGTH

The experiments presented thus far have been conducted with a constant magnetic field and the containment of electrons and ions in the plasma would therefore have been the same (apart from some variations in the electron temperature with different pressures). It is important to look at how the magnetisation of the plasma changes throughout the system as the solenoids are progressively separated from the antenna. For a 5 eV electron population, the thermal velocity is 9.4×10^5 m/s. For the field strengths discussed in this study, the electron Larmor radius is less than 1 mm near the solenoids and only becomes comparable to the radius of the tube over a meter from z_B. The ion Larmor radius, however, is much more comparable to the Echidna tube radius and it is instructive to investigate the effect of ion magnetisation.

Figure 5 shows the ion Larmor radius at the center of the antenna, $z = 0$ cm, as the solenoids are progressively moved away, i.e., as $z_B \to -60$ cm. When the solenoids are supplied with a current of 40 A (solid line), the figure shows that the Larmor radius is less than the radius of the glass tube (dotted horizontal line) for $|z_B| < 34$ cm. For $|z_B| > 34$ cm, the Larmor radius increases rapidly as the magnitude of the magnetic field strength decreases far from the solenoids.

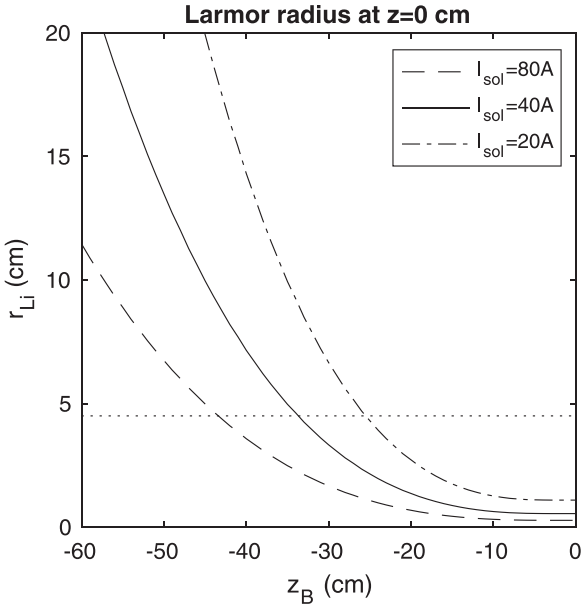

FIG. 5. The Larmor radius of ions at $z = 0$ cm due to the solenoidal field at z_B powered by currents of 20 A (dashed-dotted line), 40 A (solid line), and 80 A (dashed line). The horizontal dotted line at $r = 4.5$ cm indicates the inner radius of the Echidna chamber.

Interestingly, this value of z_B where the ion Larmor radius exceeds the glass tube radius at $z = 0$ cm is close to the value which results in the largest density on the axis in Fig. 2. As such, it is possible that ion magnetisation under the antenna determines which of the regimes discussed earlier will be observed in the axial density profiles. To test this hypothesis, the expected ion Larmor radius for stronger and weaker magnetic fields can be calculated and the cases where $I_{sol} = 20$ A and 80 A are plotted in Fig. 5. For $I_{sol} = 20$ A, the Larmor radius is doubled as the magnetic field strength is halved and the figure shows that the r_{Li} exceeds the glass tube radius at $z_B \sim 26$ cm. Similarly, for the $I_{sol} = 80$ A case, the magnetic field strength is double that of the 40 A case, halving r_{Li} and causing the point where it exceeds the tube radius to move away from the antenna to $z_B \sim 44$ cm. Given that the regime change found earlier in the $I_{sol} = 40$ A case occurred when z_B moved from -30 cm to -40 cm, a similar regime change might be observed in the $I_{sol} = 20$ A and 80 A cases when z_B moves from $z_B = -20$ cm to -30 cm and $z_B = -40$ cm to -50 cm, respectively, if ion magnetisation in the antenna region is responsible for this behavior.

To test this, the experiments which produced the axial density profiles in Fig. 2 were repeated with solenoid currents of 20 A and 80 A. Only the density profiles for values of z_B near that which would cause r_{Li} to exceed the glass tube radius at $z = 0$ cm are plotted in Fig. 6 for clarity. The $I_{sol} = 20$ A case is shown in Fig. 6(a) for z_B values of -20, -30, and -40 cm. When $z_B = -20$ cm and the ions are magnetized under the antenna, the axial density demonstrates a singly peaked profile; however, when z_B moves to -30 cm, and r_{Li} exceeds the tube radius, the profile exhibits two peaks. The density of these peaks is comparable to the $z_B = -20$ cm case; however, when z_B moves even further from the antenna, the density under the solenoid decreases by a factor of $\sim$2. Given that r_{Li} at $z = 0$ cm is expected to exceed the glass tube radius at $z_B \sim 26$ cm, the similarity between the densities in the $z_B = -20$ cm and $z_B = -30$ cm cases is not entirely surprising given that the transition from magnetized to unmagnetised ions might still be occurring. By $z_B = -40$ cm, the transition has occurred and the operating regime has well and truly changed from a singly peaked to doubly peaked density profile.

For the $I_{sol} = 80$ A case shown in Fig. 6(b), only the results for z_B values of -30, -40, -50 cm are plotted. The critical value of z_B which results in the ion Larmor radius exceeding the tube radius was $z_B \sim 44$ cm. Therefore, ions are still magnetized under the antenna in the $z_B = -30$ and -40 cm cases. The axial density profiles displayed in Fig. 6(b) for these cases are singly peaked, and the regime transition with increasing separation between antenna and solenoid has not yet occurred. When the solenoids are moved to $z_B = -50$ cm, the density profile is doubly peaked and has reduced in density nearly by a factor of 2, again aligning with the position of z_B where the ions become unmagnetised under the antenna, i.e., $z_B = -44$ cm for $I_{sol} = 80$ A.

The calculations of r_{Li} used a constant thermal velocity of 400 m/s across all magnetic field strengths. It is unlikely that this is a constant over all experimental conditions and probably varies spatially; however, the first order analysis of ion magnetisation here appears to describe the remote coupling regimes well.

VII. DISCUSSION AND CONCLUSIONS

The results and observations discussed above support the hypothesis that the operating regime changes based on the degree of ion magnetisation under the antenna. When ions are magnetized, the

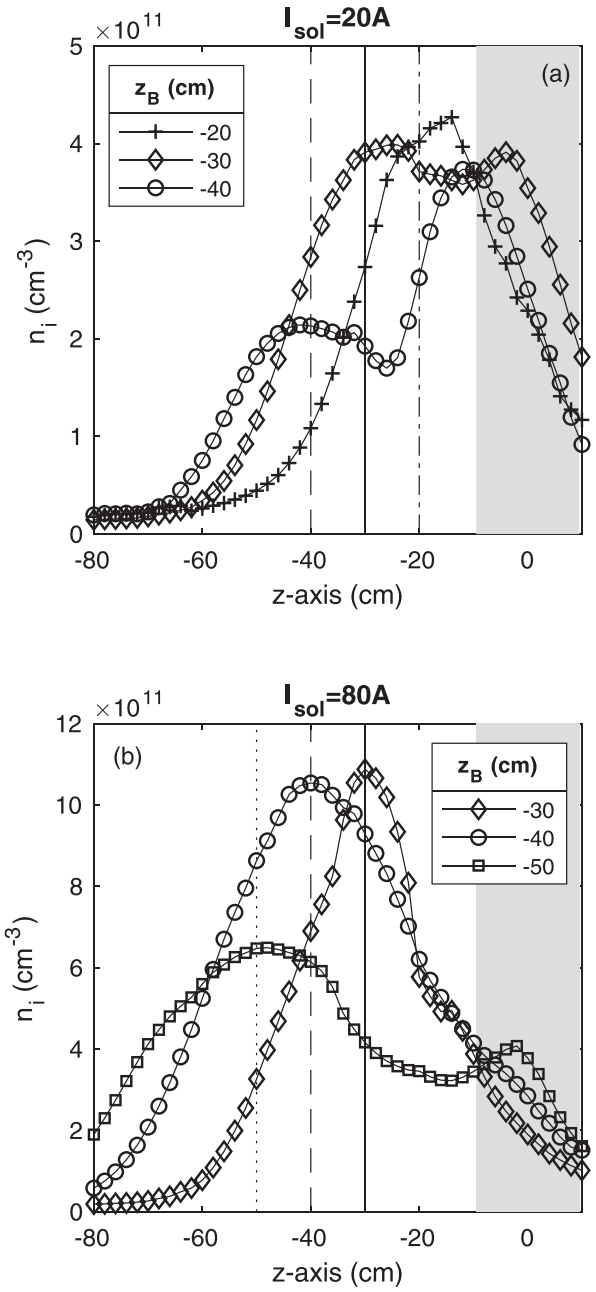

FIG. 6. Axial density measurements for different values of z_B for experimental conditions of 1 mTorr, 200 W RF power, and solenoid currents of (a) $I_{sol} = 20$ A and (b) $I_{sol} = 80$ A. The region directly under the RF antenna is shaded in gray and the solenoid location is indicated by the vertical lines for $z_B = -20$ cm (dashed-dotted), $z_B = -30$ cm (solid), $z_B = -40$ cm (dashed), and $z_B = -50$ cm (dotted).

plasma supports efficient transport of electrons from the heating region under the RF antenna to the region of high magnetic field strength. Ions themselves are not transported to the region of high magnetic field strength because the mean free path for ion-neutral charge exchange collisions is ~2.5 cm which is much smaller than the order of z_B. However, the electrons have a much larger mean free path for electron-neutral and ionizing collisions and are transported along a column defined by the magnetic field lines which pass through the antenna region. As these magnetic field lines feature a converging geometry, the column decreases in radius, thereby increasing the density of electrons on the axis. Significant charging of the radial walls enables a flat radial potential structure: the radial density profile does not follow the radial T_e profile which implies that collisions and ion gyrokinetic properties are responsible for the radial density profiles. These results appear to be independent of the argon gas pressure and RF power.

The radial walls of Echidna are an insulating glass tube and can therefore be anisotropically charged, dependent on the local equilibrium flux ratio of positive and negative particles incident on the wall. If the walls were grounded and conducting, the floating potential of the walls would be forced to be 0 V everywhere. In this particular instance in a magnetized plasma, the relationship $Vp - Vf \sim 5kT_e$ remains essentially correct; however, the absolute value of V_f is not forced to be 0 V. As electrons are more highly magnetized than ions and have longer mean free paths for elastic and inelastic collisions, the potential of the radial wall will be determined by considering the local ion flux arriving from the bulk of the local plasma and the nonlocal electron flux along the magnetic field line intersecting the wall at that location. With the solenoidal magnetic field sufficiently distant, the plasma ions under the antenna are unmagnetised and can easily drift toward the radial wall, increasing the ion flux to the radial wall under the antenna compared to the magnetized case. The build-up of positive charge on the wall attracts electrons in order to balance the flux of positive and negative charges. This would alter the cross field electron transport locally and impact the equilibrium conditions of the nonlocal electron population streaming along the magnetic field lines that intersect the antenna region. Therefore, when ions become less magnetized, the equilibrium conditions of the electron populations restricted to field lines passing through the antenna region would change. Given that these electrons are those that are heated near the antenna and transported to the region of high magnetic field, it is very likely that ion magnetisation and wall charging under the antenna play a significant role in the creation of a high density, remotely ionized plasma under the solenoids, possibly explaining the shift in the operating regime.

These results open a range of interesting avenues for future research in Echidna and similar reactors. First, if ion magnetisation is responsible for the observed behavior, then an investigation with different gases could be conducted. For gases with much higher atomic/molecular weight, the ion Larmor radius is much larger due to the increased inertia and would exceed the glass tube radius for smaller distances between the solenoids and antenna. For much lighter gases, however, the Larmor radius would be smaller, meaning that the remote ionization seen in this study could be achieved for much larger distances between the antenna and solenoids for the same magnetic field. Experiments of this kind could be conducted with xenon and helium for high and low mass gases.

An additional way to test the dependence on the magnetic field would be to study plasmas in Echidna under different magnetic field strengths and solenoid configurations. Figure 5 showed that the ion Larmor radius rapidly increases away from the solenoids and r_{Li} under the antenna is about 11.5 cm for $z_B = -60$ cm in the $I_{sol} = 80$ A case,

i.e., much larger than the glass tube. As such, with the solenoids currently installed on Echidna, the solenoid current would have to be about 200 A to bring the ion Larmor radius at $z = 0$ cm inside the glass tube when the solenoids are positioned at $z_B = -60$ cm. This would result in a maximum magnetic field > 1.5 kG; however, this is not currently possible with the DC power supply used and would overheat the solenoid coils quite quickly. Alternatively, more solenoids could be mounted on the experiment, allowing for an axially longer region of high magnetic field, potentially stretching the remotely ionized plasma.

One of the more curious results presented in this study is that the density appears to increase along the increasing magnetic field despite the large magnetic mirror ratio on the axis. The results showed that the plasma potential was maximum at the solenoids when there was strong remote coupling. As briefly discussed earlier, the acceleration of electrons toward this maximum negates the magnetic mirror effect by effectively increasing the loss angle of the magnetic mirror. These dynamics are understandable in the DC operation of Echidna; however, it remains to be seen how this axial potential structure is initiated. When no plasma is present, there would be no accelerating potential driving electrons toward z_B and the magnetic mirror would reflect incident particles. The plasma observed under the solenoids is due to local ionization and excitation as the lifetime of the excited atomic states is less than microseconds. It seems that hot electrons are transported along the field lines from the antenna region but they are additionally energized by an axial electric field that appears to approximately obey the Boltzmann equation and negate the magnetic mirror. How this potential structure is formed and how it is supported is unclear and leads to a severe "chicken and egg" problem. Therefore, a study of the plasma breakdown is necessary to understand how this system works. It is predicted here that the significant anisotropic charging of the dielectric radial walls could be responsible for setting up this DC potential structure, allowing electrons to initially overcome the magnetic mirror.

REFERENCES

[1]M. J. Burin, G. R. Tynan, G. Y. Antar, N. A. Crocker, and C. Holland, "On the transition to drift turbulence in a magnetized plasma column," Phys. Plasmas **12**(5), 052320 (2005).
[2]S. C. Thakur, M. Xu, P. Manz, N. Fedorczak, C. Holland, and G. R. Tynan, "Suppression of drift wave turbulence and zonal flow formation by changing axial boundary conditions in a cylindrical magnetized plasma device," Phys. Plasmas **20**(1), 012304 (2013).
[3]G. A. Navratil, J. Slough, and A. K. Sen, "A steady state linear machine for collisionless plasma studies," Plasma Phys. **24**(2), 185–196 (1982).
[4]D. M. Goebel, G. Campbell, and R. W. Conn, "Plasma surface interaction experimental facility (PISCES) for materials and edge physics studies," J. Nucl. Mater. **121**, 277–282 (1984).
[5]B. D. Blackwell, J. F. Caneses, C. M. Samuell, J. Wach, J. Howard, and C. Corr, "Design and characterization of the magnetized plasma interaction experiment (MAGPIE): A new source for plasma-material interaction studies," Plasma Sources Sci. Technol. **21**(5), 055033 (2012).
[6]J. Santoso, R. Manoharan, S. O'Byrne, and C. S. Corr, "Negative hydrogen ion production in a helicon plasma source," Phys. Plasmas **22**(9), 093513 (2015).
[7]C. Charles and R. Boswell, "Current-free double-layer formation in a high-density helicon discharge," Appl. Phys. Lett. **82**(9), 1356–1358 (2003).
[8]C. Charles, "Hydrogen ion beam generated by a current-free double layer in a helicon plasma," Appl. Phys. Lett. **84**(3), 332–334 (2004).
[9]S. Pottinger, V. Lappas, C. Charles, and R. Boswell, "Performance characterization of a helicon double layer thruster using direct thrust measurements," J. Phys. D: Appl. Phys. **44**(23), 235201 (2011).
[10]A. Fruchtman, K. Takahashi, C. Charles, and R. W. Boswell, "A magnetic nozzle calculation of the force on a plasma," Phys. Plasmas **19**(3), 033507 (2012).
[11]R. W. Boswell and F. F. Chen, "Helicons—The early years," IEEE Trans. Plasma Sci. **25**(6), 1229–1244 (1997).
[12]F. F. Chen and R. W. Boswell, "Helicons—The past decade," IEEE Trans. Plasma Sci. **25**(6), 1245–1257 (1997).
[13]R. W. Boswell, "Very efficient plasma generation by whistler waves near the lower hybrid frequency," Plasma Phys. Controlled Fusion **26**, 1147 (1984).
[14]F. F. Chen, "Experiments on helicon plasma sources," J. Vac. Sci. Technol., A **10**(4), 1389–1401 (1992).
[15]F. F. Chen, "Helicon discharges and sources: A review," Plasma Sources Sci. Technol. **24**(1), 014001 (2015).
[16]R. W. Boswell, E. Marsch, and C. Charles, "The current-free electric double layer in a coronal magnetic funnel," Astrophys. J. **640**(2), L199–L202 (2006).
[17]L. P. Block, "A double layer review," Astrophys. Space Sci. **55**(1), 59–83 (1978).
[18]N. Krupp, "New surprises in the largest magnetosphere of our solar system," Science **318**(5848), 216–217 (2007).
[19]Y.-M. Wang and J. Frank, "Plasma infall and X-ray production in the magnetic funnel of an accreting neutron star," Astron. Astrophys. **93**, 255–268 (1981).
[20]C. M. Samuell, B. D. Blackwell, J. Howard, and C. S. Corr, "Plasma parameters and electron energy distribution functions in a magnetically focused plasma," Phys. Plasmas **20**(3), 034502 (2013).
[21]W. D. Cox, "Magnetic steering of the ion beam in the helicon double layer thruster," Ph.D. thesis, The Australian National University, 2010.
[22]R. L. Merlino, "Understanding Langmuir probe current-voltage characteristics," Am. J. Phys. **75**(12), 1078–1085 (2007).
[23]P. Chabert and N. Braithwaite, *Physics of Radio-Frequency Plasmas* (Cambridge University Press, 2011).
[24]I. D. Sudit and F. F. Chen, "RF compensated probes for high-density discharges," Plasma Sources Sci. Technol. **3**(2), 162–168 (1994).
[25]V. Godyak, R. Piejak, and B. Alexandrovich, "Measurements of electron energy distribution in low-pressure RF discharges," Plasma Sources Sci. Technol. **1**, 36–58 (1992).
[26]K. Takahashi, C. Charles, R. W. Boswell, T. Kaneko, and R. Hatakeyama, "Measurement of the energy distribution of trapped and free electrons in a current-free double layer," Phys. Plasmas **14**(11), 114503 (2007).
[27]V. I. Demidov, S. V. Ratynskaia, R. J. Armstrong, and K. Rypdal, "Probe measurements of electron energy distributions in a strongly magnetized low-pressure helium plasma," Phys. Plasmas **6**(1), 350–358 (1999).
[28]V. A. Godyak and V. I. Demidov, "Probe measurements of electron-energy distributions in plasmas: What can we measure and how can we achieve reliable results?," J. Phys. D: Appl. Phys. **44**, 233001 (2011).
[29]V. A. Godyak, R. B. Piejak, and B. M. Alexandrovich, "Probe diagnostics of non-Maxwellian plasmas," J. Appl. Phys. **73**(8), 3657–3663 (1993).
[30]R. F. Kemp and J. M. Sellen, "Plasma potential measurements by electron emissive probes," Rev. Sci. Instrum. **37**(4), 455–461 (1966).
[31]T. A. Lafleur, "Helicon wave propagation in low diverging magnetic fields," Ph.D. thesis, Australian National University, 2011.
[32]G. G. Borg and R. C. Cross, "Guided propagation of Alfven and ion-ion hybrid waves in a plasma with two ion species," Plasma Phys. Controlled Fusion **29**(6), 681–696 (1987).
[33]A. W. Degeling, C. O. Jung, R. W. Boswell, and A. R. Ellingboe, "Plasma production from helicon waves," Phys. Plasmas **3**(7), 2788 (1996).
[34]F. F. Chen, *Introduction to Plasma Physics and Controlled Fusion* (Plenum Press, 1984).
[35]T. Lafleur, C. Charles, and R. W. Boswell, "Plasma control by modification of helicon wave propagation in low magnetic fields," Phys. Plasmas **17**(7), 073508 (2010).